Actin Filament Dynamics in Living Glial Cells Imaged by Atomic Force Microscopy

E. Henderson,* P. G. Haydon, D. S. Sakaguchi

Observation of filamentous actin (F-actin) in living cells is currently limited to the resolution of the light microscope. Higher resolution procedures require sample fixation and preclude dynamic studies. The atomic force microscope (AFM) can image and manipulate samples at very high, sometimes atomic resolution by scanning a fine tip over the surface of interest and detecting physical interactions between the tip and sample. This study demonstrates that F-actin can be readily resolved in living cells with the AFM and that the dynamic properties of F-actin are easily observed.

The cytoskeleton is a dynamic structural framework fundamental to cell function. Filamentous actin is a major constituent of the cytoskeleton and plays important roles in cell motility, regulation of cell shape, and intracellular transport (*1*). Previous work has shown that the AFM (*2*) can be used to explore biological processes and structures, including fixed and living cells (*3*, *4*). We studied the cytoskeletal network in living cells with the AFM. An amphibian cell line was isolated from *Xenopus laevis* retinal neuroepithelium (*5*). This cell line, designated XR1, has been characterized as a glial cell line on the basis of the immunocytochemical localization of glial cell markers such as glial fibrillary acidic protein and vimentin. The XR1 cells support neurite outgrowth and deposit an extracellular matrix that is also capable of promoting axonal outgrowth.

To begin a detailed analysis of surface features with the AFM, we plated XR1 glial cells on glass cover slips that were coated with collagen or a basement membrane preparation composed primarily of entactin, collagen, and laminin (ECL). Live XR1 glial cells were imaged in growth media. Typical images collected in two different modes at applied vertical imaging forces between 10 and 30 nN are shown in Fig. 1. Transient increases in imaging force as the scanning tip encountered a rapid change in topography were as high as 12 nN, producing total imaging forces of 42 nN. Images collected in height mode (Fig. 1A) provide precise information regarding surface topography and produce accurate three-dimensional (3-D) images of the cell (*6*). In contrast, data collected in error signal mode (Fig. 1B) emphasize changes in elevation (similar to a first derivative of a height mode image), thereby providing images that have fine surface detail but lack quantitative height information (*7*). In many cases, only portions of the cells were observed because the cells are frequently larger than the maximum field size (132 μm by 132 μm).

After XR1 cells have attached to the substrate, they begin spreading to achieve a relatively flattened morphology. The margins of the cultured glial cells are similar to migrating neuronal growth cones and are comprised of lamellae of two distinct forms: (i) a lamellipodium at the cell margin that spreads and attaches in a flattened form to the substrate and (ii) filopodia, spike-like protrusions that also arise from the cell margin. Changes in these morphological features and additional changes in internal structures over time clearly indicated that the cells were alive during imaging with the AFM. A series of images collected over 40 min is shown in Fig. 2. The edge of the XR1 glial cell underwent obvious morphological changes during this time period. Filamentous structures that displayed dynamic properties were commonly observed. For example, the spacing between two filaments (arrowheads at 8 and 16 min in Fig. 2) increased by 3 μm in 8 min.

Confocal laser scanning microscopy of individual identified cells after AFM imaging, fixation, and rhodamine-phalloidin staining demonstrated that the filaments observed with the AFM were, in fact, actin filaments (Fig. 3A). Treatment of the cells with cytochalasin B, a fungal toxin that inhibits actin polymerization, resulted in a change in morphology that included loss of the filamentous structures (Fig. 3B). Fluorescence staining indicated that both the lamellipodia and the filopodia contain F-actin and microtubules (β-tubulin). However, microtubules apparently contributed little to the filamentous structures observed by the AFM. Double-labeling studies with rhodamine-phalloidin and monoclonal antibodies to β-tubulin demonstrated that tubulin is more concentrated in the perinuclear region of the cells. Confocal microscopy indicated that microtubules generally

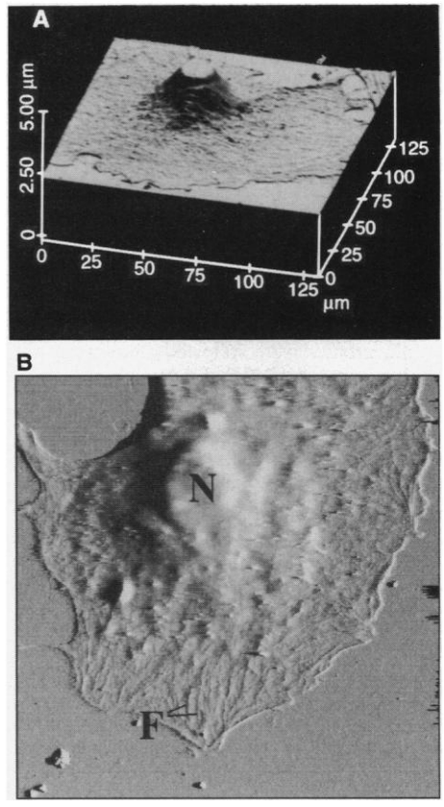

Fig. 1. AFM images of living XR1 glial cells. (**A**) AFM image of an XR1 cell collected in an imaging mode in which the true height of the specimen is revealed (height mode). The 3-D presentation, in which the cell is artificially illuminated at a 30° angle from behind, illustrates this capability. In this example, a portion of the nucleus is saturated because its height exceeded the *z*-axis detection limit. The field size is 132 μm by 132 μm. (**B**) AFM image of an XR1 cell collected in error signal mode, an imaging mode that emphasizes surface detail of the specimen but lacks the precise height information provided by height mode. N, nucleus; F, filament. The field size is 85 μm by 85 μm. Unless otherwise noted, applied vertical imaging forces were typically 10 to 30 nN [based on cantilever spring constant values supplied by Digital Instruments (Santa Barbara, California)]. Transient force increases were as high as 12 nN above the applied vertical equilibrium force. The AFM used was a Nanoscope III (Digital Instruments). Cantilevers were commercial 200-μm silicon nitride (Digital Instruments) with integral pyramidal tips and spring constants estimated to be 0.12 N per meter by the manufacturer. We prepared substrates by coating acid-washed, 12-mm glass cover slips with collagen (rat tail; Sigma) or ECL (Upstate Biotechnology, Inc., Lake Placid, New York) at a final concentration of 5 μg/ml. XR1 glial cells were then plated on these coated cover slips at a density of 4000 cells per milliliter. Glial cells were cultured in L-15 medium (60%) (Sigma) supplemented with fetal bovine serum (10%) and Fungibact (1%) (Sigma).

Department of Zoology and Genetics, Signal Transduction Training Group, Iowa State University, Ames, IA 50011.

*To whom correspondence should be addressed.

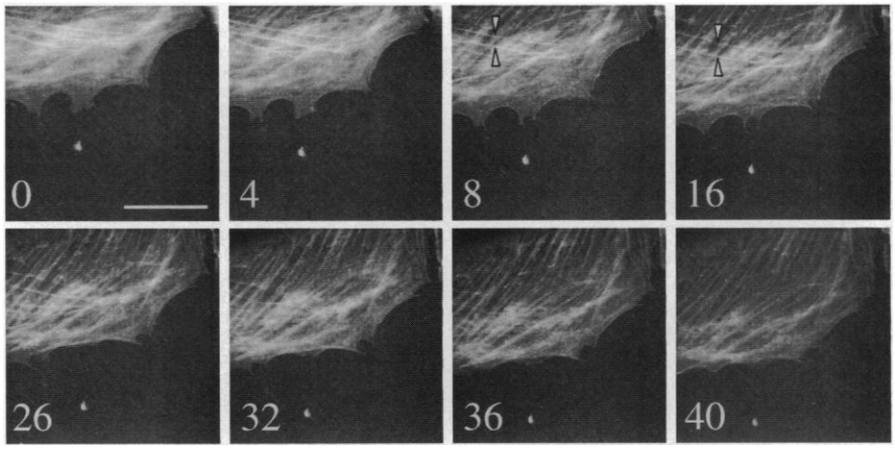

Fig. 2. Temporal sequence of AFM images of an XR1 glial cell. Over the 40-min time course shown, many changes in the morphology of the edge of the cell as well as of internal filaments (F-actin) are apparent. Arrowheads in the 8- and 16-min time frames indicate the position at which an increase of 3 μm in the spacing between two filaments occurred in an 8-min period. Some drift occurred during image acquisition so that more of the cell was observed at later times. The white spot below the cell edge was a fortuitous static positional marker, and true cell movement can be determined relative to this marker. Data was collected in height mode. Scale bar = 50 μm.

lie beneath actin filaments in these cells. Thus, it is possible that they are hidden from the AFM scanning tip by the overlying actin filament networks. Moreover, microtubules may be more susceptible to perturbation by the scanning tip than F-actin and therefore may be difficult to detect under the imaging forces used.

The AFM can image actin filaments through the plasma membrane without apparent damage to the cell. Images of subsurface cellular features may be obtained by the AFM in several ways. For instance, the surface of the plasma membrane may conform to the shape of the underlying rigid filaments (Fig. 4A). In this case, the scanning tip would follow the plasma membrane surface contours, creating a topographical map of the cytoskeletal elements close to the surface. The limit of resolution would then be a function of the pliability and thickness of the plasma membrane, and individual F-actin filaments within actin bundles may therefore be obscured.

A second possibility is that the scanning tip penetrates the fluid membrane during imaging (Fig. 4B). For instance, the force necessary to perturb a Langmuir-Blodgett (LB) film by the AFM has been calculated to be less than 1 nN (*8*); the applied vertical forces used in this study were between 10 and 30 nN, well above this limit. The plasma membrane is significantly more robust than an LB film and may be able to withstand considerably higher imaging forces. However, we find that after depolymerization of F-actin by treatment with cytochalasin B, the remaining membrane appears fragile and highly susceptible to perturbation by the scanning tip (Fig. 3B), which suggests that the underlying filaments were reinforcing the membrane and that in their absence the scanning tip easily disrupts it. Thus, it is formally possible that the AFM scanning tip penetrates the plasma membrane while imaging and that the underlying cytoskeleton helps maintain cell integrity

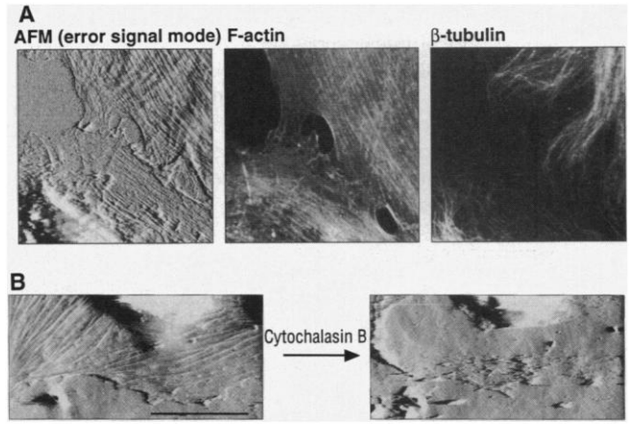

Fig. 3. Filaments revealed by the AFM correspond to F-actin. In (**A**) a pair of glial cells was imaged by the AFM (left panel) and confocal laser scanning microscopy (middle and right panels). The filaments in the live XR1 glial cell imaged by the AFM correspond to those in the F-actin image (rhodamine-phalloidin stained), but not to those in the β-tubulin image (stained by antibody to β-tubulin) in the same cells after fixing (*9*). The time between AFM imaging and fixation, as well as perturbation of the cell structure by the fixation process, results in some morphological differences in the living (AFM) and fixed cell images. The field size is 85 μm by 85 μm. (**B**) AFM images of an XR1 cell before (left) and immediately after (within 4 min) addition of cytochalasin B, a compound that inhibits actin polymerization (*9*). Note the apparent sensitivity of the remaining membrane (right) to the force applied by the scanning tip after loss of actin filaments. Scale bar = 50 μm.

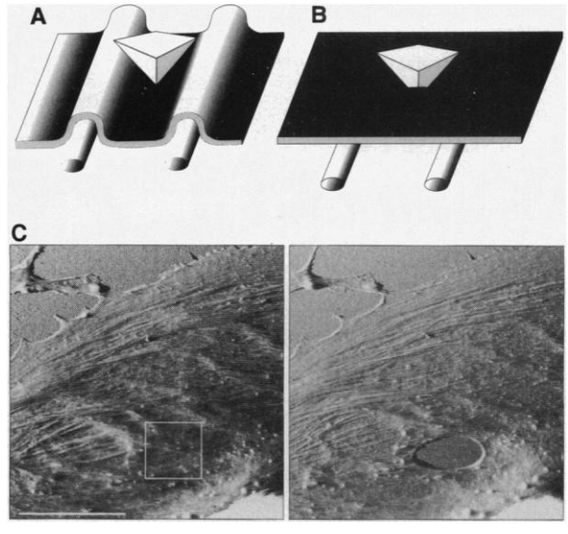

Fig. 4. The compliance or fluidity of the plasma membrane is important for imaging internal structures in living cells by the AFM. Imaging mechanisms that would reveal cytoskeletal features in living cells include (**A**) the membrane deformation model and (**B**) the membrane penetration model. In (A), the plasma membrane is flexible and conforms to the contours of the underlying cytoskeleton. The scanning tip (pyramid) does not directly contact the cytoskeleton in this model. In (B), the scanning tip penetrates the plasma membrane and contacts the cytoskeletal elements below. (**C**) AFM images of a living glial cell, illustrating the ability of the cell membrane to reseal after "nanosurgery" by the scanning tip. A force of >100 nN was applied to the cell in a square raster pattern in the area indicated by the white box in the image on the left. Subsequent imaging with a smaller force (10 nN) revealed that the cell was still viable, and the hole generated by the scanning tip apparently sealed around the edges, maintaining cellular integrity. Data were collected in error signal mode. Scale bar = 50 μm.

during this process. Application of a large imaging force (applied vertical force >100 nN) to a selected region of a living cell produced a hole in the cell without jeopardizing cell viability (Fig. 4C). This "nanosurgery" experiment was readily reproducible. The hole may result from fusion of the two bilayers under pressure from the AFM tip and cannot be taken as direct evidence of a single bilayer penetration mechanism. Nonetheless, these data show that a living cell can withstand severe perturbation of the plasma membrane by the scanning tip, a quality that may prove very useful in future studies of living cells by the AFM.

Although the AFM is considered a surface probe, it is capable of imaging subsurface features such as F-actin within living cells. The AFM can collect 3-D data and is capable of higher resolution imaging than conventional optical microscopes on many surfaces. If this resolving capability can be realized with living cells, the AFM should prove a powerful tool for the investigation of dynamic interactions between cell surface and subsurface structures, a critical step in many signal transduction pathways.

REFERENCES AND NOTES

1. S. J. Smith, *Science* **242**, 708 (1988).
2. G. Binnig, C. F. Quate, C. Gerber, *Phys. Rev. Lett.* **56**, 930 (1986).
3. S. A. C. Gould *et al.*, *J. Vac. Sci. Technol. A* **8**, 369 (1990); E. Henderson, *Nucleic Acids Res.* **20**, 445 (1992); J. H. Hoh, R. Lal, S. A. John, J.-P. Revel, M. F. Arnsdorf, *Science* **253**, 1405 (1991); B. Drake *et al.*, *ibid.* **243**, 1586 (1989); H. J. Butt *et al.*, *J. Struct. Biol.* **105**, 54 (1990); C. Bustamante *et al.*, *Biochemistry* **31**, 22 (1991); H. J. Butt, K. H. Downing, P. K. Hansma, *Biophys. J.* **58**, 1473 (1990); V. Parpura, personal communications.
4. R. D. Edstrom *et al.*, *FASEB J.* **4**, 3144 (1990); O. Marti *et al.*, *J. Microsc.* **152**, 803 (1988); C. A. J. Putman *et al.*, *Ultramicroscopy*, in press; T. Tomie *et al.*, *Science* **252**, 691 (1991); J. Vesenka *et al.*, *Ultramicroscopy*, in press; J. Vesenka *et al.*, *SPIE Proc.* **1639**, 38 (1992); A. L. Weisenhorn *et al.*, *Scanning Electron Microsc.* **4**, 511 (1990); A. L. Weisenhorn *et al.*, *Biophys. J.* **58**, 1251 (1990); A. L. Weisenhorn *et al.*, *Langmuir* **7**, 8 (1991); D. Keller *et al.*, *SPIE Proc.* **1639**, 91 (1992).
5. D. S. Sakaguchi *et al.*, *Dev. Biol.* **134**, 158 (1989).
6. J. H. Hoh and P. K. Hansma, *Trends Cell Biol.* **2**, 208 (1992).
7. C. A. J. Putnam *et al.*, *Rev. Sci. Instrum.* **63**, 1914 (1992).
8. M. Radmacher, R. M. Zimmermann, H. E. Gaub, in *The Structure and Conformation of Amphiphilic Membranes*, R. Lipowski, D. Richter, K. Kremer, Eds. (Springer Proceedings in Physics, Springer-Verlag, Berlin, 1992), vol. 66, pp. 24–29.
9. Cultures were rinsed with phosphate-buffered saline (PBS) and fixed in 4% paraformaldehyde in a 0.1 M PO_4 buffer at 22°C for 1 to 2 hours. The cultures were rinsed in PBS, blocked for 30 min in PBS plus 5% goat serum, and incubated in primary antibodies overnight at 4°C. They were then rinsed in PBS and incubated with fluorescently conjugated secondary antibodies for 90 min, rinsed again, and mounted on glass microscope slides. Primary antibodies were diluted in PBS that contained 0.3% Triton X-100 (Sigma). The antibody to β-tubulin (E7, from M. Klymkowsky) was diluted 1:20. Fluorescent secondary antibody (fluorescein isothiocyanate–conjugated goat antibody to mouse; Fisher Scientific, Springfield, NJ) was diluted 1:150 in PBS. Cultures were incubated with rhodamine-phalloidin (1:30) in 0.3% Triton X-100 in PBS for 30 min after the incubations in the secondary antibodies in the dark at room temperature. Cultures were then rinsed three times in PBS and mounted on glass microscope slides with Gelmount (Fisher). Fluorescence was detected with an Odyssey confocal laser scanning microscope (Noran Instruments, Middleton, WI). For the cytochalasin B sensitivity experiment, cytochalasin B (Sigma, dissolved at a final concentration of 20 mM in dimethyl sulfoxide) was diluted to 10 μM with growth medium. During scanning, the cytochalasin B was added from the side with a fine glass needle to the AFM fluid cell (Digital Instruments) in which the O-ring seal had been omitted. Approximately 10 μl of cytochalasin B solution was added to the 200-μl imaging chamber to give a final concentration of ~0.5 μM. Addition of the cytochalasin B took approximately 30 s; the image shown (Fig. 3B, right panel) was acquired immediately after cytochalasin B addition for a total time course of approximately 4.5 min. The ports in the fluid cell were not used to avoid detrimental hydrodynamic effects on image acquisition and cell adhesion.

10. We thank M. Klymkowsky for antibody to β-tubulin, V. Parpura for developing and sharing AFM imaging methods for living cells, and K. Radke for expert technical assistance. The authors are members of the Signal Transduction Training Group at Iowa State University supported by NSF. Supported by a grant from the Iowa State University Biotechnology Council (D.S.S.) and by NIH and NSF (E.H. and P.G.H.). P.G.H. is an Alfred P. Sloan Fellow.

23 April 1992; accepted 8 July 1992

Multiple Zinc Finger Forms Resulting from Developmentally Regulated Alternative Splicing of a Transcription Factor Gene

Tien Hsu, Joseph A. Gogos, Susan A. Kirsh,* Fotis C. Kafatos†

Transcripts encoding the *Drosophila* putative transcription factor CF2 are subject to developmentally regulated alternative splicing, and they encode protein isoforms that differ in the number of zinc fingers. One testis-specific RNA encodes an isoform that includes three zinc fingers and a frame-shifted segment. Two other transcripts encode isoforms with six and seven zinc fingers which bind to distinct promoters and DNA target sequences. Thus, because of alternative splicing, a single gene appears to encode distinct DNA-binding proteins, each capable of regulating different gene sets in different tissues and developmental periods.

Transcription factors can serve as developmental switches, that is, they turn specific sets of genes on or off at appropriate locations and at different times during development (*1*). Transcription factors cannot be regulated only by transcription, because such regulation would require an infinity of factors. Their posttranscriptional modulation occurs by alternative splicing (*2*), intracellular compartmentalization (*3*), interaction with inhibitors (*4*), translational regulation (*5*), or posttranslational modification such as phosphorylation (*6*). We now present evidence that posttranscriptional regulation of a Cys_2-His_2 zinc finger factor can occur by alternative splicing within the DNA-binding domain, thus utilizing the modularity of

T. Hsu, J. A. Gogos, S. A. Kirsh, Department of Cellular and Developmental Biology, Harvard University, Cambridge, MA 02138.
F. C. Kafatos, Department of Cellular and Developmental Biology, Harvard University, Cambridge, MA 02138, and also the Institute of Molecular Biology and Biotechnology, FORTH and Department of Biology, University of Crete, Heraklion 711 10, Crete, Greece.

*Present address: Department of Molecular Biology, Massachusetts General Hospital, Boston, MA 02114.
†To whom correspondence should be addressed.

Fig. 1. Nucleotide sequence of the *CF2* gene coding strand and derived amino acid sequences. Exon sequences are numbered consecutively from the first of three mRNA 5′ ends (·) detected by primer extension (*8*). In the 5′ untranscribed region, the TATA box (ATATA) and a partial match to the CF2-I protein binding consensus (TATATTATA) are shown in upper case; bold lower case indicates nucleotides flanking the consensus, which are encompassed in CF2-I protein footprints (Fig. 3B). Portions of the intron sequences near the splice junctions are shown in lower case but not numbered. (↘) indicates splice donor and (→↘) splice acceptor sites. Possible zinc finger motifs in the peptide sequences are underlined, and designations (f1, f2) on the left mark their beginnings. The additional line of peptide sequence (italicized) from position 1505 on is the frame-shifted CF2-III peptide. Arrows above the nucleotide sequence indicate the oligonucleotide primers used in PCR reactions (Fig. 2, C and D). Underlined residues in the 3′ untranslated region indicate possible polyadenylation signals, which are consistent with the 3′ ends of cDNA clones (vertical arrow heads) and the results of S1 protection assays (*8*). The designations for amino acid residues are in the standard single-letter code: A, Ala; C, Cys; D, Asp; E, Glu; F, Phe; G, Gly; H, His; I, Ile; K, Lys; L, Leu; M, Met; N, Asn; P, Pro; Q, Gln; R, Arg; S, Ser; T, Thr; V, Val; W, Trp; and Y, Tyr.